Front. Phys. 13(4), 137306 (2018)
https://doi.org/10.1007/s11467-018-0784-0

RESEARCH ARTICLE

Evolution of individual quantum Hall edge states in the presence of disorder

Kai-Tong Wang[1], Fuming Xu[2], Yanxia Xing[3,†], Hong-Kang Zhao[1,‡]

[1] *School of Physics, Beijing Institute of Technology, Beijing 100081, China*
[2] *Shenzhen Key Laboratory of Advanced Thin Films and Applications, College of Physics and Energy, Shenzhen University, Shenzhen 518060, China*
[3] *Beijing Key Laboratory of Nanophotonics and Ultrafine Optoelectronic Systems, School of Physics, Beijing Institute of Technology, Beijing 100081, China*
Corresponding authors. E-mail: †*xingyanxia@bit.edu.cn,* ‡*zhaohonk@bit.edu.cn*
Received February 1, 2018; accepted March 14, 2018

By using the Bloch eigenmode matching approach, we numerically study the evolution of individual quantum Hall edge states with respect to disorder. As demonstrated by the two-parameter renormalization group flow of the Hall and Thouless conductances, quantum Hall edge states with high Chern number n are completely different from that of the $n = 1$ case. Two categories of individual edge modes are evaluated in a quantum Hall system with high Chern number. Edge states from the lowest Landau level have similar eigenfunctions that are well localized at the system edge and independent of the Fermi energy. On the other hand, at fixed Fermi energy, the edge state from higher Landau levels exhibit larger expansion, which results in less stable quantum Hall states at high Fermi energies. By presenting the local current density distribution, the effect of disorder on eigenmode-resolved edge states is distinctly demonstrated.

Keywords quantum Hall edge states, Landau level, quantum phase transition

PACS numbers 73.23.-b, 73.43.Nq, 72.10.Bg, 73.50.-h

1 Introduction

Integer quantum Hall effect (IQHE) has gained intensive research attention since it was proposed in 1980 [1]. Unlike the mono-gapped systems such as quantum anomalous Hall (QAH) and quantum spin Hall (QSH) systems, the band structure of IQHE system is multi-gapped, which is characterized by high Chern number n. Consequently, the quantum phase transition of IQHE is of particular interest, such as the metal-insulator transition (MIT) [2, 3]. To study the transition behavior of quantum Hall (QH) states, the two-parameter scaling theory was proposed [4, 5], and numerical investigations were performed on a QH system to verify the two-parameter flow [6, 7]. Besides, the global phase diagram [8] of IQHE predicted that no direct transition from general QH states to insulator appeared under the effect of perturbations or disorders for the high occupation case. However, later experiments [9–11] and theories[12–14] indicated that direct MIT of $n > 1$ QH state was achievable.

All of the prominent features of MIT in QH systems are owing to the presence of multiple edge states at the device's boundaries [15, 16]. These edge states originate from different Landau levels induced by an external magnetic field, and the number of edge states equals the Chern number n. Unlike the QAH chiral edge states and QSH helical edge states [17, 18], QH edge states are robust against any type of disorder, static or spin-dependent. During the metal-insulator transition of QH states, edge states from different Landau levels respond distinctly to disorder, and these gapped Landau levels are closely linked through edge states. Therefore, the effect of disorder on edge states from different Landau levels remains an interesting matter, and the underlying mechanism attracts our research interest. For simplicity, the QH states discussed here and afterwards all refer to IQHE.

In this study, we first investigate the two-parameter renormalization group (RG) flow of QH states in 2-dimensional lattice system based on a supercell system

[19–22]. The renormalization group flow for the $n = 2$ Landau level is completely different from that of $n = 1$, suggesting the interesting MIT feature of QH systems with high Chern number. To study the phase transition of QH systems, we calculate the Hall and Thouless conductances [7, 23–25] within the lattice gauge [7]. Numerical results confirm that the $n > 1$ QH state directly transforms into insulator but the critical transition disorder strength is smaller than the case of $n = 1$. Furthermore, by adopting non-equilibrium Green's function (NEGF) formalism [26] and Bloch eigenmode matching approach [27–29], we calculate the eigenmode-resolved transmission coefficient of individual QH edge states with respect to disorder. The results show that probability distributions of edge states from the lowest Landau level are always localized at the lattice edge despite of the variation of Fermi energy, which maintains the robustness and stability of these edge states against disorder. Further, the edge state originating from higher Landau levels exhibits larger expansion across the system and they are more sensitive to disorder. The quality of QH states at the same high Chern number with different Fermi energy is also discussed. Demonstrating the local current density distributions, the evolution of individual edge states with respect to disorder is intuitively displayed.

The rest of the paper is organized as follows. In Section 2, the theoretical formalisms are introduced, and we derive the transmission coefficients and the local current density for the propagating modes. Section 3 contains the numerical results with discussions regarding our study. Finally, a brief summary is presented in Section 4.

2 Model and formalism

In this section, the system Hamiltonian and related numerical formalisms are introduced.

2.1 Hall and Thouless conductances

For a two-dimensional square lattice with external magnetic field, the Hamiltonian is expressed as [30]

$$H = \sum_{\boldsymbol{i}} \epsilon_{\boldsymbol{i}} d_{\boldsymbol{i}}^{\dagger} d_{\boldsymbol{i}} - t \sum_{\langle \boldsymbol{i},\boldsymbol{j} \rangle} \mathrm{e}^{\mathrm{i}\phi_{ij}} d_{\boldsymbol{i}}^{\dagger} d_{\boldsymbol{j}} + H.c. \tag{1}$$

where $d_{\boldsymbol{i}}^{\dagger}/d_{\boldsymbol{i}}$ is the creation/annihilation operator for an electron on site $\boldsymbol{i}$, and $\langle \boldsymbol{i},\boldsymbol{j} \rangle$ denotes the nearest neighboring lattice sites. The random on-site potential $\epsilon_{\boldsymbol{i}}$ is uniformly distributed in the interval $[-W/2, W/2]$ where W is the disorder strength, known as the Anderson-type disorder. t is the nearest-neighbor coupling strength, which is set as the unit of energy and disorder in the calculation. In the presence of a perpendicular magnetic field, an extra phase is induced in the adjacent coupling, which is defined as $\phi_{ij} = \frac{e}{\hbar}\int_i^j \boldsymbol{A}\cdot \mathrm{d}\boldsymbol{l}$ with $\boldsymbol{A}$ the magnetic vector potential. In the numerical implementation, two different gauges are adopted. For the eigenmode-resolved transmission through a ribbon system, we choose the Coulomb gauge and the vector potential is simply $\boldsymbol{A} = [-By, 0, 0]$ in Cartesian coordinate. To calculate the Hall and Thouless conductances, we use the lattice gauge with special treatment on the lattice edge [7], which allows the reduction of the system size for a fixed magnetic field. In the calculation, the extra phase through unit lattice measures the magnetic field strength. The spin degree of freedom is not considered in this study.

To calculate the transverse Hall conductance g_H, it is straightforward to adopt the relation between g_H and the total Chern number:

$$g_H = \frac{e^2}{h}\sum_n c_n, \tag{2}$$

where c_n is the Chern number of the nth band and the summation is over all the bands below the Fermi energy. The Chern number defined in k space can be written as [23, 31–33]

$$c_n = \frac{1}{2\pi \mathrm{i}}\int_{BZ} \mathrm{d}^2 k \nabla \times \boldsymbol{A'}$$

with $\boldsymbol{A'} = \langle \psi_{nk}|\partial|\psi_{nk}\rangle$ the Berry connection [34–36] and ψ_{nk} the normalized wave function of the nth Bloch band.

The longitudinal conductance can be measured by the band sensitivity subject to change in boundary conditions [25, 37]. For a disordered system, Thouless and Edwards [25, 37] proposed a relation between the average longitudinal conductance and the band curvature at the Fermi energy, which is called the Thouless conductance. At Fermi energy E_f, the Thouless conductance is expressed as [7, 23]

$$g_T(E_f) = \frac{e^2}{h}\left\langle \left| \frac{\pi}{\Delta(E_f)} \frac{\partial^2 E_f}{\partial k_x^2} \right| \right\rangle, \tag{3}$$

where $\frac{\partial^2 E_f}{\partial k_x^2}$ denotes the band curvature at E_f and $\Delta(E_f)$ is the mean level spacing. The angle bracket stands for ensemble averaging over the disorder and $|\ldots|$ refers to taking the absolute value. Since both g_H and g_T are in unit of $\frac{e^2}{h}$, the unit is omitted in the numerical results shown below.

2.2 Local current density and eigenmode-resolved Transmission coefficients

For the lattice Hamiltonian H shown in Eq. (1), based on the Green's function formalism [38–40] and the definition of current density [41, 42], the differential local current density vector at zero temperature reads

$$\mathrm{d}\boldsymbol{J}_{x/y}/\mathrm{d}(eV) = \frac{1}{2}e(\hat{\rho}\hat{v} + \hat{v}\hat{\rho}) \tag{4}$$

with

$$\hat{\rho} = \frac{1}{2\pi}\boldsymbol{G}^r\boldsymbol{\Gamma}_s\boldsymbol{G}^a,$$
$$\hat{v} = -\frac{\mathrm{i}}{\hbar}[\boldsymbol{r}, \boldsymbol{H}],$$

where $\hat{\rho}$ is the non-equilibrium density matrix and $\hat{v}$ denotes the velocity matrix in the scattering region. $\boldsymbol{\Gamma}_s = \mathrm{i}(\boldsymbol{\Sigma}_s^r - \boldsymbol{\Sigma}_s^a)$ is the linewidth function and $\boldsymbol{\Sigma}_s^r$ denotes the retarded self energy of source lead $\boldsymbol{s}$, which can be generally calculated using the transfer matrix method [43, 44].

To distinguish different propagating modes, we employ the mode matching technique [27, 28, 45, 46]. For a system divided into slices with onsite Hamiltonian H_0 and hopping Hamiltonian H_1, the Bloch equation is written as

$$(K_0 + K_1\mathrm{e}^{\mathrm{i}k_n} + K_{-1}\mathrm{e}^{-\mathrm{i}k_n})\psi_n = 0, \tag{5}$$

where $K_a = H_a - ES_a$ $(a = 0, \pm 1)$, S is the overlap matrix and ψ_n denotes the eigenvector of the nth eigenmode. Solving this equation, we can separate the right-going and left-going modes. Selecting the propagating modes and substituting them into Eq. (4), the linewidth function Γ_s becomes

$$\Gamma_s = \sum_{s_n} Q_{s_n}\frac{1}{v_{s_n}}Q_{s_n}^\dagger \tag{6}$$

with

$$Q_{s_n} = \boldsymbol{G}_{00}^{r-1}\psi_{s_n},$$
$$v_{s_n} = \mathrm{i}\frac{a}{\hbar}(\psi^\dagger K_1\psi\mathrm{e}^{\mathrm{i}ka} - \mathrm{e}^{-\mathrm{i}ka}\psi^\dagger K_{-1}\psi).$$

Similarly, the eigenmode-resolved transmission coefficient can be written as

$$T_{\alpha_m,\beta_n} = |t_{\alpha_m,\beta_n}|^2, \tag{7}$$

where t_{α_m,β_n} is the transmission matrix element. Parameters α, β, and m, n label the leads and modes, respectively. The transmission matrix element t_{α_m,β_n} is calculated from [27, 28]

$$t_{\alpha_m,\beta_n} = \sqrt{|v_{\alpha_m}|}\tilde{\psi}_{\alpha_m}^\dagger\boldsymbol{G}_{\alpha\beta}^r Q_{\beta_n}\frac{1}{\sqrt{|v_{\beta_n}|}}. \tag{8}$$

Here $\boldsymbol{G}_{00}^r$ is the Green's function of an infinite ribbon. The eigenvector ψ_m satisfies the orthonormalization condition $\tilde{\psi}_n^\dagger\psi_m = \delta_{n,m}$. v_{α_m} is the group velocity of injecting or outgoing electrons of the mth eigenmode in lead α. Detailed numerical procedures can be found in relevant references cited above.

3 Numerical results and discussion

To investigate the critical behavior in the topological phase transition, we calculate the two-parameter renormalization group (RG) flow of Hall conductance g_H and Thouless conductance g_T driven by the system size. In the presence of disorder, discrete Landau levels are broadened into Landau bands. A critical energy appears in the center of the Landau band, supporting an extended state and separating adjacent QH phases [7]. Adopting the lattice gauge, the extra phase per unit lattice associated with the magnetic field is set as $\phi = 2\pi/9$. The corresponding RG flows are shown in Fig. 1. In Fig. 1(a), we plot the RG flow related to the first Landau level, where the flow links the zeroth and the first QH states with $g_H = 0$ and $g_H = 1$, respectively. The arrows show the behaviors of g_T and g_H as the system size increases. Evidently, g_T always decreases with the increase of the system size. On the contrary, the Hall conductance decays to $g_H = 0$ at the left and grows to $g_H = 1$ at the right. As a result, a transition point corresponding to the critical energy emerges in the middle of the flow map, which is typical for mono-gapped topological insulators. The numerical results in Fig. 1(a) are perfectly consistent with previous theoretical predictions [4, 5]. Further, the RG flow corresponding to the second Landau level ($n = 2$) shown in Fig. 1(b) is severely unsymmetric between $g_H = 1$ and $g_H = 2$. The critical transition point severely deviates from the flow center but is close to the $g_H = 1$ QH state. The deviation and difference in Fig. 1(b) indicate that the RG flow from the first Landau level is more robust against the disorder. Furthermore, these numerical results indicate that the quality of different Landau levels is not the same, which will have an impact on the evolution of QH states

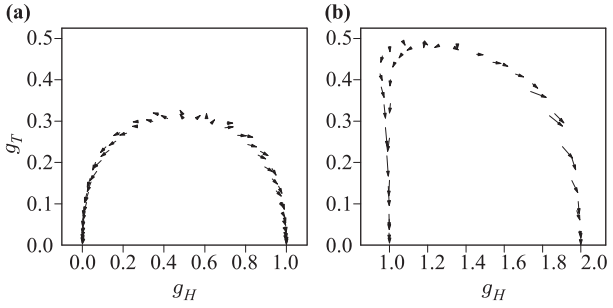

Fig. 1 The renormalization group flows extracted from finite size scaling, with system size ranging from wid=12 to 27 and disorder strength $W \in [1, 1.5]$ for magnetic field $\phi = 2\pi/9$. The arrows indicate the increase in system size. The flows in **(a)** and **(b)** correspond to Landau levels $n = 1$ and $n = 2$, respectively. The numerical results are averaged over 10 000 random configurations.

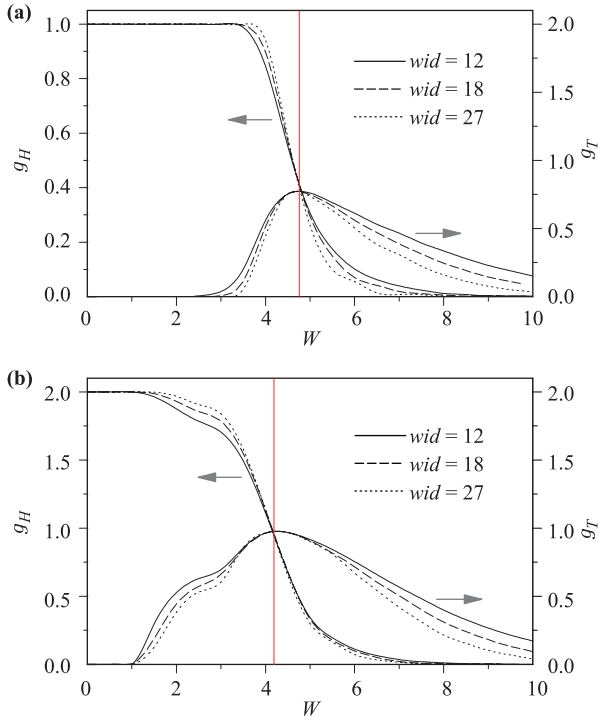

Fig. 2 Hall conductance g_H and Thouless conductance g_T versus disorder strength W for different system sizes. **(a)** and **(b)** correspond to Fermi energies $E_f = -3$ and $E_f = -2$, which are located in the $n = 1$ and $n = 2$ QH plateaus, respectively. The red dashed lines indicate the critical transition disorder strengths $W_1 = 4.7$ and $W_2 = 4.2$. The magnetic field is fixed at $\phi = 2\pi/9$.

at metal-insulator transition (MIT) in the presence of disorder.

To explore the transition behaviors of the QH states from conductor to insulator, we investigate the evolution of Hall and Thouless conductances with disorders at fixed magnetic field $\phi = 2\pi/9$. The Fermi energy is first set as $E_f = -3$, which is located at the center of the $n = 1$ QH plateau. The ensemble averaged Hall and Thouless conductances versus disorder strength W are shown in Fig. 2. At weak disorder, the Hall conductance is perfectly quantized as $g_H = 1$ and the Thouless conductance is zero. With the increase of disorder strength, g_H is rapidly reduced and eventually becomes zero, and g_T quickly increases to maximum and then gradually decreases. For different system sizes, all g_H curves cross at a critical disorder point as indicated by the red dashed line in Fig. 2(a). Meanwhile, the maximal Thouless conductances appear at the same disorder, which are independent of system sizes. Except this critical point, the averaged g_T depends on the system size and demonstrates the behavior of localized states at large disorder [47, 48]. The critical disorder strength at $E_f = -3$ is $W_1 = 4.7$, which characterizes MIT of QH states. In Fig. 2(b), we plot the dependence of g_H and g_T on the disorder strength W at $E_f = -2$, which labels the $n = 2$ QH states. Similar behaviors of g_H and g_T are observed, and we also find a critical disorder strength $W_2 = 4.2$ as shown by the red dashed line in Fig. 2(b). The results prove that the $n = 2$ QH states can directly transform to insulator without intermediate QH state. Besides, the critical transition disorder strength will decrease with the increase of Chern number, which means high QH states are more vulnerable to disorder. Together with the renormalized group flow shown in Fig. 1, the properties of high QH states are more significant since there are multi edge states originating from multi-gapped Landau levels. Therefore, to demonstrate the evolution of individual edge states in the presence of disorder, we will intuitively visualize the edge states and show the eigenmode-resolved transmission.

In real space, QH states display as a series of edge states in the system with finite size. The destruction of these edge states owing to disorder causes the metal-insulator transition. To intuitively visualize the edge states, we calculate the local current density for the $n = 1$ and $n = 2$ QH states and presnt the numerical results in Fig. 3. The lattice system under investigation has width $wid = 54$ and magnetic field $\phi = 2\pi/9$. In Figs. 3(a) and (c), we plot the local current density of QH states for energy $E_f = -3$ ($n = 1$) and $E_f = -2$ ($n = 2$) with disorder strength $W = 0$. Evidently, the $n = 1$ and $n = 2$ QH states are perfectly localized at the upper edge of the lattice and no current density exists in the bulk, which

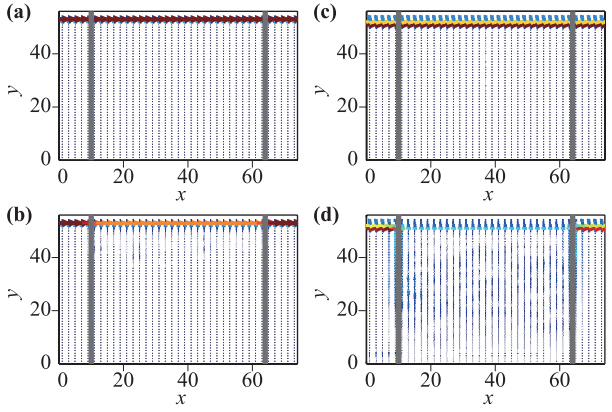

Fig. 3 Local differential current density distributions for both $n = 1$ and $n = 2$ QH states with fixed magnetic field $\phi = 2\pi/9$. The arrow at the lattice site denotes the direction of the density vector and its length indicates the density magnitude. The color of arrow changing from blue (light) to red (dark) refers to the increase in magnitude. Other parameters in each panel: **(a)** $E_f = -3$ and $W = 0$; **(b)** $E_f = -3$ and $W = 2$; **(c)** $E_f = -2$ and $W = 0$; **(d)** $E_f = -2$ and $W = 2$. The width of the system is $wid = 54$ lattices and x is the transport direction. The results are averaged over 10 000 configurations.

is the signature of edge states. An obvious difference between the density patterns of two QH states is that the $n = 2$ state has a larger expansion in y-direction, which is double-degenerate with $g_H = 2$. When introducing disorder in the lattice, the local current density of both edge states are shown in Figs. 3(b) and (d) with the same disorder strength $W = 2$. The results are obtained via averaging over 10 000 random configurations. It is evident that both edge states are affected by the disorder. The edge-moving electrons injected from the clean lead are scattered into the bulk of the central scattering region. The thick black lines indicate the border between the clean leads and the disordered region. Comparing Figs. 3(b) and (d), we find that the $n = 1$ QH state still exhibits a major edge portion with small density distribution in the entire scattering region. On the other hand, the edge state of $n = 2$ is almost completely destroyed under the same disorder. We can confirm from these numerical results that the edge state of $n = 1$ QH state is more robust than the $n = 2$ QH state. Hence, a larger critical MIT disorder is expected for lower QH state. The $n = 2$ QH state has double-degenerate edge states, which belong to the 1st and 2nd Landau levels, respectively.

To further understand the properties of edge states associated with different Landau levels, we separate the degenerate edge states and investigate them individually for the high occupation case with Chern number $n > 1$. In Fig. 4, the band structure of a QH system is presented. The lattice under investigation has width $wid = 40$ with magnetic field $\phi = 2\pi/20$. Due to the magnetic field, the original parabolic spectrum becomes highly degenerated and transforms to discrete Landau levels as shown in the figure. The edge states cross the gaps and link adjacent

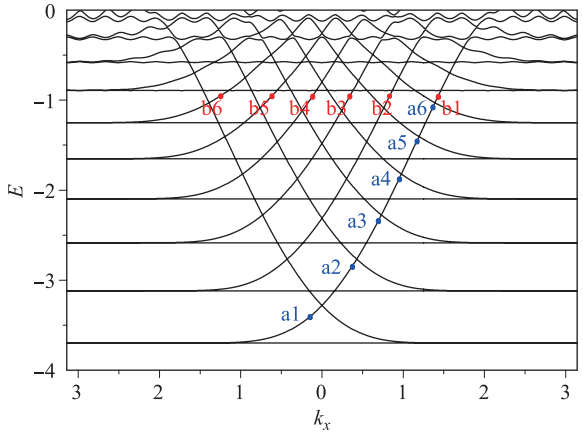

Fig. 4 The band structure of a lattice system in clean limit with magnetic field $\phi = 2\pi/20$ and width $wid = 40$. The blue points (a1–a6) correspond to the same Landau level in different gaps, and the red points (b1–b6) belong to different Landau levels at the same Fermi energy $E_f = -0.95$.

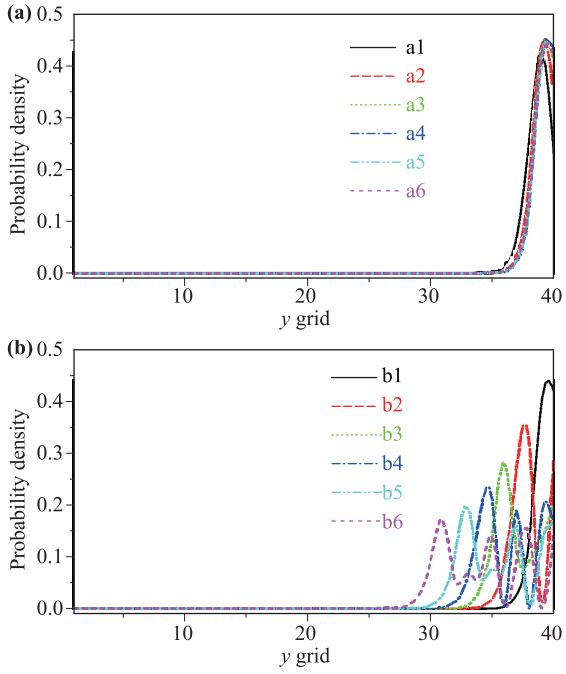

Fig. 5 The probability density distributions of edge states corresponding to the crossed points in Fig. 4. **(a)** Density distributions of edge states from the lowest Landau level, and the Fermi energies lie in the center of each gap. **(b)** Density distributions of edge states from different Landau levels with the same Fermi energy $E_f = -0.95$. The lattice width is $wid = 40$.

Landau levels. The edge state gradually emerges when scanning Fermi energy over the energy band. These edge states are classified into two distinct categories. At high Fermi energy such as $E_f = -0.95$, six individual edge states exist, which are labeled as red points from b1 to b6. Among these edge states, b1 comes from the first Landau level, while b6 from the sixth. Since all the Landau levels are gapped and linked, these edge states may exhibit different characteristics. On the other hand, the blue points (from a1 to a6) are selected from the same Landau level (the lowest) but located in the center of different gaps with various injecting energies. The edge qualities of these two categories will be intensively studied in the following part. Notice that these energy points are non-degenerate.

In Fig. 5, we present the lattice probability densities of two series of edge states, the blue points a1–a6 and the red points b1–b6 in Fig. 4. The probability densities of the blue points, i.e., edge states from the same Landau level with different energies are plotted in Fig. 5(a). The result indicates that in the absence of disorder, edge states from the lowest Landau level for different Fermi energies demonstrate the same behavior and exhibit almost identical distributions. The eigenfunctions are strictly restrained on the boundary, acting

as edge modes. On the contrary, in Fig. 5(b), the probability densities of edge states from different Landau levels with the same energy $E_f = -0.95$ exhibit distinct distributions. Evidently, the density distribution of the eigenmode from the lowest Landau level is perfectly localized at the lattice edge as indicated by the black solid line. Starting from b2, node(s) will appear in the eigenfunction of edge states and local minimums emerge in the probability distributions in Fig. 5(b). With the increase in Chern number n, the probability distribution gradually spreads into the lattice center, which implies that the quality of corresponding edge state decays. For instance, the density distribution corresponding to b6 edge state expands to one fourth of the lattice in y-direction. These numerical facts reveal the generic difference between edge states from the two categories. In the following, we will demonstrate the properties of these edge states in the presence of disorder, accompanied with local differential current density distributions defined in Eq. (4).

Using the mode matching method, we are able to study the properties of individual edge states against disorder. Specifically, the eigenmode-resolved transmission coefficient T of each propagating mode and its current density distribution in the lattice can be numerically calculated. We first study the evolution of individual edge modes from the first Landau level with different energies. We focus on the lowest 6 gaps shown by blue points in Fig. 4. Here, the injecting energy is set at the center of each gap. The eigenmode-resolved transmission coefficients for different energies versus disorder strength W are shown in Fig. 6(a). As illustrated in Fig. 5(a), the eigenfunctions of edge states from the same Landau level are nearly identical. However, from Fig. 6(a), we can observe that these edge states respond differently to large disorders. The eigenmode-resolved T satisfies the order $T_{a1} > T_{a2} > T_{a3} > T_{a4} > T_{a5} > T_{a6}$ in the entire disorder range. We also plot the local differential current density distributions with different energies in Figs. 6(b) and (c). It is evident that at the same disorder $W = 1.5$, the edge state with lowest energy persists well, and the $6th$ edge mode has been destructed in the central scattering region. Since the energy gap between adjacent Landau levels gradually becomes narrower at high occupation, the edge state from the same Landau level with higher energy is more vulnerable to disorder.

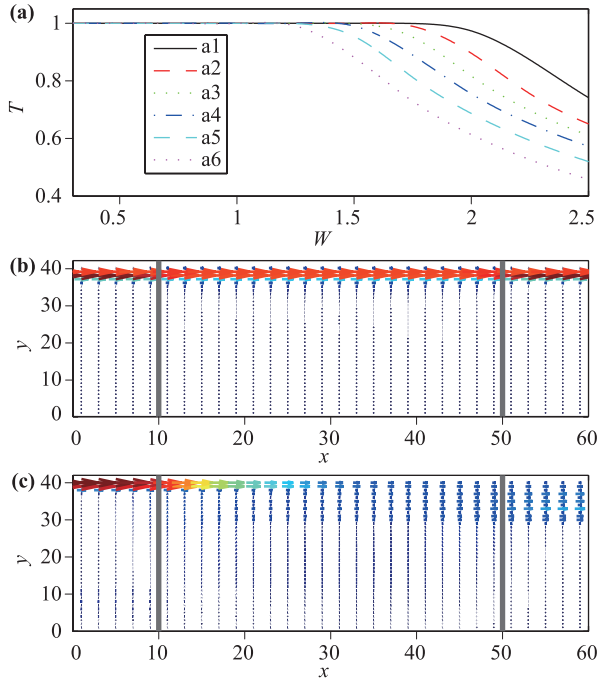

Fig. 6 **(a)** plots the eigenmode-resolved transmission coefficients versus disorder for the first Landau level, with Fermi energies located at the center of different gaps, as indicated by blue points (a1–a6) in Fig. 4; **(b)** and **(c)** are the local differential current density distributions corresponding to edge states in the $1st$ and $6th$ gaps with disorder strength $W = 1.5$. The magnetic field is $\phi = 2\pi/20$ and the lattice has width $wid = 40$, which are same as in Fig. 4.

Finally, we set the Fermi energy at fixed values and investigate edge modes from the same QH state. The $n = 6$ QH states with two Fermi energies are evaluated and the eigenmode-resolved transmission coefficient T versus disorder strength W are presented in Fig. 7(a). The data are obtained by averaging over 10 000 configurations. Here we have selected two Fermi energies, $E_{f1} = -1.07$ (gray lines) and $E_{f2} = -0.95$ (color lines), which are at the center and top edge of the 6th energy gap, respectively. For weak disorder, all transmission coefficients are ideally quantized as $T = 1$. With the increase of disorder, the eigenmode-resolved T starts to decrease gradually. A notable contrast is that the resolved transmissions at E_{f1} are always larger than that at E_{f2} for the same disorder, which suggests that with the same high Chern number the QH state at the gap center is more robust than that close to the top edge of the same gap. Another intuitive fact is that for both E_{f1} and E_{f2}, the order $T_{b1} > T_{b2} > T_{b3} > T_{b4} > T_{b5} > T_{b6}$ at the same W is observed in the entire disorder window. This fact indicates that, for the same Fermi energy, the resolved edge state of a lower Landau level is more stable than that of a higher Landau level. This result is consistent with the conclusion in Fig. 5(b), since the edge state from a higher Landau level has larger expansion and is more easily affected by disorder. It is noticeable that, the resolved T for the QH state at the top gap edge (color lines) is more easy to be distinguished from each other than those for the QH state at gap center (gray lines), suggesting that MIT of this sensitive QH state is primarily caused by the edge states from high Landau levels. In Figs. 7(b) and (c), we show the local current density

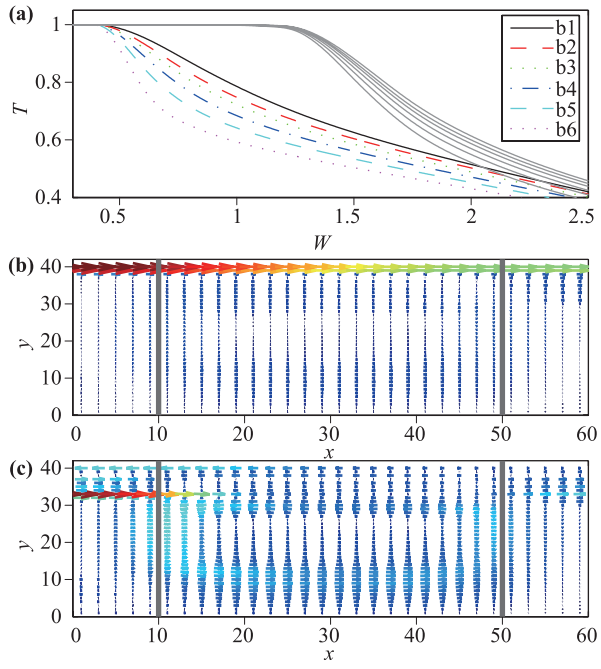

Fig. 7 **(a)** shows the eigenmode-resolved transmission coefficients as a function of the disorder strength W for fixed Fermi energies $E_{f1} = -1.07$ (grey lines) and $E_{f2} = -0.95$ (color lines), respectively. $T_{\rm b1} > T_{\rm b2} > T_{\rm b3} > T_{\rm b4} > T_{\rm b5} > T_{\rm b6}$ is observed in the entire disorder window for both Fermi energies. **(b)** and **(c)** are the local differential current density distributions of eigenmodes corresponding to the 1st and 5th Landau levels of the $n = 6$ QH state with $E_f = -0.95$ and disorder strength $W = 0.7$. Other parameters are same as in Fig. 6.

distributions of edge states b1 and b5 for $E_{f2} = -0.95$ of the $n = 6$ QH state. In the clean lead ($x \in [0, 10]$), the 1st edge state is sharply localized at the lattice edge and the 5th one has a larger expansion in y-direction. In the scattering region with the same disorder $W = 0.7$, the 1st edge mode is well preserved while the 5th edge mode is destroyed and spread in the entire region. These evidences distinctly show that for the QH state with high Chern number, the edge state from higher Landau level is less stable.

4 Conclusion

In summary, we have studied the evolution of edge states in disordered two-dimensional quantum Hall systems. The two-parameter renormalization group flow shows that the QH state with high Chern number $n > 1$ is completely different from that of the state with $n = 1$. Adopting non-equilibrium Green's function formalism and Bloch eigenmode matching approach, the evolution of eigenmode-resolved edge states with respect to disorder is studied in detail. We have verified that, for the lowest Landau level, the edge states injecting from different band gaps exhibit similar probability distributions. For a quantum Hall state at fixed Fermi energy with multiple edge states, the edge state from a lower Landau level is more localized at the system edge, and always more robust against disorder. On the contrary, the edge modes from higher Landau levels exhibit larger expansion across the system, and are more sensitive to disorder. Furthermore, the quality of QH states with the same high Chern number significantly depends on the Fermi energy. When E_f is at the top gap edge, the eigenmode-resolved transmission is more easy to be distinguished from each other than the gap center case. Presenting the local current density distributions, the evolution of eigenmode-resolved edge states in the presence of disorder is intuitively visualized.

Acknowledgements This work was financially supported by the National Natural Science Foundation of China (Grant Nos. 11674024 and 11504240). F. Xu acknowledges support from Shenzhen Key Lab Fund (Grant No. ZDSYS 20170228105421966).

References

1. K. V. Klitzing, G. Dorda, and M. Pepper, New method for high-accuracy determination of the fine-structure constant based on quantized Hall resistance, *Phys. Rev. Lett.* 45(6), 494 (1980)
2. A. Bao, Y. H. Chen, H. F. Lin, H. D. Liu, and X. Z. Zhang, Quantum phase transitions in two-dimensional strongly correlated fermion systems, *Front. Phys.* 10(5), 106401 (2015)
3. F. Evers and A. D. Mirlin, Anderson transitions, *Rev. Mod. Phys.* 80(4), 1355 (2008)
4. A. M. M. Pruisken, Universal singularities in the integral quantum Hall effect, *Phys. Rev. Lett.* 61(11), 1297 (1988)
5. D. E. Khmel'nitskii, Quantization of Hall conductivity, *Pis'ma Z. Eksp. Teor. Fiz.* 38, 454 (1983) [*JETP Lett.* 38(9), 552 (1983)]
6. J. Song, and E. Prodan, Characterization of the quantized Hall insulator phase in the quantum critical regime, *Eur. Phys. Lett.* 105(3), 37001 (2014)
7. M. A. Werner, A. Brataas, F. von Oppen, and G. Zaránd, Anderson localization and quantum Hall effect: Numerical observation of two-parameter scaling, *Phys. Rev. B* 91(12), 125418 (2015)
8. S. Kivelson, D. H. Lee, and S. C. Zhang, Global phase diagram in the quantum Hall effect, *Phys. Rev. B* 46(4), 2223 (1992)
9. S. H. Song, D. Shahar, D. C. Tsui, Y. H. Xie, and D. Monroe, New universality at the magnetic field driven

insulator to integer quantum Hall effect transitions, *Phys. Rev. Lett.* 78(11), 2200 (1997)

10. T. Wang, K. P. Clark, G. F. Spencer, A. M. Mack, and W. P. Kirk, Magnetic-field-induced metal-insulator transition in two dimensions, *Phys. Rev. Lett.* 72(5), 709 (1994)
11. S. V. Kravchenko, W. Mason, J. E. Furneaux, and V. M. Pudalov, Global phase diagram for the quantum Hall effect: An experimental picture, *Phys. Rev. Lett.* 75(5), 910 (1995)
12. D. N. Sheng and Z. Y. Weng, New universality of the metal-insulator transition in an integer quantum Hall effect system, *Phys. Rev. Lett.* 80(3), 580 (1998)
13. D. N. Sheng and Z. Y. Weng, Phase diagram of the integer quantum Hall effect, *Phys. Rev. B* 62(23), 15363 (2000)
14. X. C. Xie, D. Z. Liu, B. Sundaram, and Q. Niu, Transition from the integer quantum Hall state to the insulator state, *Phys. Rev. B* 54(7), 4966 (1996)
15. B. I. Halperin, Quantized Hall conductance, current-carrying edge states, and the existence of extended states in a two-dimensional disordered potential, *Phys. Rev. B* 25(4), 2185 (1982)
16. M. Büttiker, Absence of backscattering in the quantum Hall effect in multiprobe conductors, *Phys. Rev. B* 38, 9375 (1988)
17. Y. Ren, Z. Qiao, and Q. Niu, Topological phases in two-dimensional materials: A review, *Rep. Prog. Phys.* 79(6), 066501 (2016)
18. Y. Ren, J. Zeng, K. Wang, F. Xu, and Z. Qiao, Tunable current partition at zero-line intersection of quantum anomalous Hall topologies, *Phys. Rev. B* 96(15), 155445 (2017)
19. Q. Niu, D. J. Thouless, and Y. S. Wu, Quantized Hall conductance as a topological invariant, *Phys. Rev. B* 31(6), 3372 (1985)
20. Y. Hatsugai, K. Ishibashi, and Y. Morita, Sum rule of Hall conductance in a random quantum phase transition, *Phys. Rev. Lett.* 83(11), 2246 (1999)
21. A. M. Essin and J. E. Moore, Topological insulators beyond the Brillouin zone via Chern parity, *Phys. Rev. B* 76(16), 165307 (2007)
22. Y. Y. Zhang, R. L. Chu, F. C. Zhang, and S. Q. Shen, Localization and mobility gap in the topological Anderson insulator, *Phys. Rev. B* 85(3), 035107 (2012)
23. Z. G. Song, Y. Y. Zhang, J. T. Song, and S. S. Li, Route towards localization for quantum anomalous Hall systems with Chern number 2, *Sci. Rep.* 6(1), 19018 (2016)
24. K. Nomura, S. Ryu, M. Koshino, C. Mudry, and A. Furusaki, Quantum Hall effect of massless Dirac fermions in a vanishing magnetic field, *Phys. Rev. Lett.* 100(24), 246806 (2008)
25. J. T. Edwards, and D. J. Thouless, Numerical studies of localization in disordered systems, *J. Phys. C* 5(8), 807 (1972)
26. J. S. Wang, B. K. Agarwalla, H. Li, and J. Thingna, Nonequilibrium Green's function method for quantum thermal transport, *Front. Phys.* 9(6), 673 (2014)
27. P. A. Khomyakov, G. Brocks, V. Karpan, M. Zwierzycki, and P. J. Kelly, Conductance calculations for quantum wires and interfaces: Mode matching and Green's functions, *Phys. Rev. B* 72(3), 035450 (2005)
28. T. Ando, Quantum point contacts in magnetic fields, *Phys. Rev. B* 44(15), 8017 (1991)
29. L. Zhang, Y. Xing, and J. Wang, First-principles investigation of transient dynamics of molecular devices, *Phys. Rev. B* 86(15), 155438 (2012)
30. Y. Xing, Q. F. Sun, and J. Wang, Influence of dephasing on the quantum Hall effect and the spin Hall effect, *Phys. Rev. B* 77(11), 115346 (2008)
31. T. Fukui and Y. Hatsugai, Quantum spin Hall effect in three dimensional materials: Lattice computation of Z_2 topological invariants and its application to Bi and Sb, *J. Phys. Soc. Jpn.* 76(5), 053702 (2007)
32. T. Fukui, Y. Hatsugai, and H. Suzuki, Chern numbers in discretized Brillouin zone: Efficient method of computing (spin) Hall conductances, *J. Phys. Soc. Jpn.* 74(6), 1674 (2005)
33. T. Fukui and Y. Hatsugai, Topological aspects of the quantum spin-Hall effect in graphene: Z_2 topological order and spin Chern number, *Phys. Rev. B* 75(12), 121403 (2007)
34. D. J. Thouless, M. Kohmoto, M. P. Nightingale, and M. den Nijs, Quantized Hall conductance in a two-dimensional periodic potential, *Phys. Rev. Lett.* 49(6), 405 (1982)
35. M. V. Berry, Quantal phase factors accompanying adiabatic changes, *Proc. R. Soc. Lond. A* 392(1802), 45 (1984)
36. B. Simon, Holonomy, the quantum adiabatic theorem, and Berry's phase, *Phys. Rev. Lett.* 51(24), 2167 (1983)
37. D. Braun, E. Hofstetter, A. MacKinnon, and G. Montambaux, Level curvatures and conductances: A numerical study of the Thouless relation, *Phys. Rev. B* 55(12), 7557 (1997)
38. A. P. Jauho, N. S. Wingreen, and Y. Meir, Time-dependent transport in interacting and noninteracting resonant-tunneling systems, *Phys. Rev. B* 50(8), 5528 (1994)
39. Y. Xing, J. Wang, and Q. F. Sun, Focusing of electron flow in a bipolar graphene ribbon with different chiralities, *Phys. Rev. B* 81(16), 165425 (2010)
40. J. Li and S. Q. Shen, Spin-current-induced charge accumulation and electric current in semiconductor nanostructures with Rashba spin-orbit coupling, *Phys. Rev. B* 76(15), 153302 (2007)

41. H. Jiang, L. Wang, Q. F. Sun, and X. C. Xie, Numerical study of the topological Anderson insulator in HgTe/CdTe quantum wells, *Phys. Rev. B* 80(16), 165316 (2009)

42. Y. Xing, L. Zhang, and J. Wang, Topological Anderson insulator phenomena, *Phys. Rev. B* 84(3), 035110 (2011)

43. D. H. Lee and J. D. Joannopoulos, Simple scheme for surface-band calculations (II): The Green's function, *Phys. Rev. B* 23(10), 4997 (1981)

44. D. H. Lee and J. D. Joannopoulos, Simple scheme for surface-band calculations (I), *Phys. Rev. B* 23(10), 4988 (1981)

45. S. Sanvito, C. J. Lambert, J. H. Jefferson, and A. M. Bratkovsky, General Green's-function formalism for transport calculations with spd Hamiltonians and giant magnetoresistance in Co- and Ni-based magnetic multilayers, *Phys. Rev. B* 59(18), 11936 (1999)

46. I. Rungger and S. Sanvito, Algorithm for the construction of self-energies for electronic transport calculations based on singularity elimination and singular value decomposition, *Phys. Rev. B* 78(3), 035407 (2008)

47. T. Ando, Electron localization in a two-dimensional system in strong magnetic fields (I): Case of short-range scatterers, *J. Phys. Soc. Jpn.* 52(5), 1740 (1983)

48. T. Ando, Electron localization in a two-dimensional system in strong magnetic fields (II): Long-range scatterers and response functions, *J. Phys. Soc. Jpn.* 53(9), 3101 (1984)